RSC Applied Polymers

ROYAL SOCIETY OF CHEMISTRY

PAPER

View Article Online
View Journal

Cite this: DOI: 10.1039/d6lp00046k

Honeycomb-patterning in soft polymer networks: using geometry to manipulate toughness and failure

Alyssa VanZanten, †[a] Emily England,†[a] Aditya Ketkar,[a] Cooper Priest,[a] Surbhi Punhani-Schillinger,[a] Hongwei Wu,[b] Giuseppe Buscarnera,[b] Michelle M. Driscoll [c] and Caroline R. Szczepanski *[a]

Received 7th February 2026,
Accepted 25th May 2026

DOI: 10.1039/d6lp00046k

rsc.li/rscapplpolym

Hexagonal (*i.e.* honeycomb) patterning has been previously shown to increase overall material toughness as a function of geometry when the base lattice material is brittle in nature. However, similar design parameters have yet to be identified for soft materials such as polymer networks that are viscoelastic in nature. Here, systematic stress–strain experiments of honeycomb-patterned lattice sheets based in poly(ethylene glycol) explore the failure behavior as a function of honeycomb geometry as well as base material rigidity. Experimental results demonstrate that geometry impacts Young's modulus and alters failure mode and toughness differently than previously observed in other material classes. Specifically, honeycomb structures of smaller dimensions enhance tortuosity during crack propagation while also allowing for rotations and deformations that dissipate stress, enabling simultaneous enhancement of toughness and strength.

1. Introduction

Soft materials have distinct behaviors compared to traditional elastic solids,[1] mainly they can withstand larger deformations than brittle glasses and plastics. Polymer networks, comprised of polymer chains connected by cross-linking junctions, thus forming a three dimensional structure[2] represent a subset of soft materials that are particularly attractive for emerging applications in biomedicine (*i.e.*, tissue engineering, medical devices),[3] agriculture,[4] and soft robotics.[5] This is largely due to the large number of functional units available to build polymer networks, and thus the ease with which critical properties such as interactions with the surrounding environment can be tailored. However, a major and persistent challenge with soft polymer networks is a lack of toughness.[2,6] These networks can suffer from catastrophic and severe failure, including self-rupture during swelling[7–9] as well as transient instabilities such as creasing, buckling and wrinkling.[10,11] Given the diverse applications for soft materials and polymer networks, understanding how to manipulate and tailor failure modes and instabilities is critical for advanced engineering applications.

Patterning is one strategy to manipulate material failure and response.[12–14] This is particularly attractive for soft materials as photo-lithography and additive manufacturing are becoming increasingly accessible tools for tailoring patterning and even creating unique structures including composite and meta-materials.[15–17] Lattice structures, such as honeycomb motifs, have been of particular interest when patterning soft materials, as this type of perforated structure has the added benefit of enhanced strength-to-weight performance.[13,14,18,19] This type of design, which consists of packed hexagonal porous domains, is seen in a number of natural systems,[20] most famously in natural honeycomb found in bees nests.[21] Recent investigations highlight how honeycomb lattices enhance stability of structural materials[22,23] as well as failure of acrylic polymer composites. Specifically, honeycomb patterning enhances crack tortuosity during tensile deformation; this is significant when compared to samples comprised of square-shaped pores.[24] This enhancement is attributed to stress distribution around the porous features, and more specifically that crack propagation in honeycomb lattices encounter a 'fork', where adjacent struts oriented 60° from the crack site can serve as a propagation site. Thus, more stochastic propagation of a crack arises. However, the precise role of hexagonal geometry (pore size, strut dimensions, *etc.*) on the extent of tortuosity and mitigation of rapid failure events have yet to be determined. Thus, it remains unclear if further enhancements

[a]*Department of Chemical Engineering & Materials Science, Michigan State University, East Lansing, Michigan 48824, United States. E-mail: szcz@msu.edu*
[b]*Department of Civil and Environmental Engineering, Northwestern University, Evanston, Illinois 60208, USA*
[c]*Department of Physics & Astronomy, Northwestern University, Evanston, Illinois 60208, United States*
† These authors contributed equally to the work.

to deformation can be engineered *via* straight-forward manipulations to pattern dimensions including pore density, strut (*i.e.* ligament) size, *etc.* (see, Fig. 1).

The systematic investigation into pattern geometry and the associated impact on failure here is motivated by prior works investigating brittle solids which identify direct links between failure mode and lattice geometric factors such as strut thickness and underlying rigidity of the base material.[13,25,26] Using these handles, failure mechanisms can be tailored from brittle cracking (*i.e.*, a quickly growing crack that travels perpendicularly across a lattice structure) to more diffuse, system-spanning breaking that exhibits tortuosity. These investigations into honeycomb pattern specific relationships, however, focused on systems where the base material is plastic or elastic in nature.

Similar design principles that enable manipulation of fracture behavior based on material patterning and geometry have yet to be identified for soft, viscoelastic materials. Compared to plastics and brittle solids, soft materials pose advantages as they can provide low energetic cost mods of deformation, such as rotation and distortion. This is particularly relevant, as distortions and rotations are observed as a means to mitigate stress in perforated, lattice systems.[25] Furthermore, prior investigations into lattice-patterned soft polymer networks, including hydrogels, demonstrate performance enhancements.[27–30] As one example, variations in vintile-lattice geometry resulted in enhancements of both Young's and shear moduli of a poly(ethylene glycol) hydrogel; decreasing unit cell size corresponded to increased modulus.[27] Similarly, investigations on photopolymer lattices fabricated *via* 3-D printing highlight how compressive strength, *i.e.* energy absorption capacity, varies based on a uniform or graded lattice geometry.[30] This body of work is motivated by emerging application fields for soft meta-materials, including wearable sensors and soft robotics.[29] As outlined above, previous investigations highlight enhancements in material properties; pattern-performance relationships are still needed for soft materials in tension so crack propagation and failure may be predicted *a priori*. Furthermore, current lattice-patterning strategies for soft materials focus on singularly enhancing either strength or toughness.[29] By investigating tensile deformation and failure in a soft material platform, new rules for failure mitigation and synergistic performance enhancement, *i.e.* addressing strength *vs.* toughness trade-offs, may arise. We hypothesize that more significant architectural enhancements to failure mode and toughness are accessible in soft materials as a function of lattice geometry, particularly when compared to examples in brittle solids and plastics, as they can exhibit more significant nonlinear deformations prior to failure.

Here we investigate the failure behavior of two-dimensional, honeycomb-patterned poly (ethylene glycol) polymer networks. The rigidity of the underlying material was varied *via* cross-link density of the formed polymer network (*i.e.* ratio of poly (ethylene glycol) diacrylate – PEGDA to poly(ethylene glycol) monoether acrylate – PEGMEA – Fig. S1). Furthermore, the hexagonal patterning was varied. Three distinct pore sizes (*i.e.*, length across the pore) and strut widths were explored (Fig. 1), resulting in 9 patterns employed (Table 1). The stress–strain behavior as a function of base material rigidity and patterning was evaluated *via* tensile testing. With honeycomb patterning, a transition from brittle to diffuse failure was observed, as expected and seen in prior reports. More interestingly, a trend emerged at low pore size where increases in strain at break and yield stress were observed with imposed patterning. In the most extreme scenarios, patterning could result in a simultaneous 10-fold increase in toughness along with a 50% increase in strength. These enhancements compared to the bulk, non-patterned control represent a strategy to improve toughness and mechanical integrity of viscoelastic materials.

2. Experimental

2.1 Materials

To develop polymer samples, the following chemicals were employed (Fig. S1): poly(ethylene glycol) methyl ether acrylate (PEGMEA) with a molecular weight of 400 g mol^{-1} was utilized as the base monomer, poly(ethylene glycol) diacrylate (PEGDA) with a molecular weight of 700 g mol^{-1} was used as the network cross-linker, and 2,2-dimethoxy-2-phenylacetophenone (DMPA) was used as the photoinitiator in all formu-

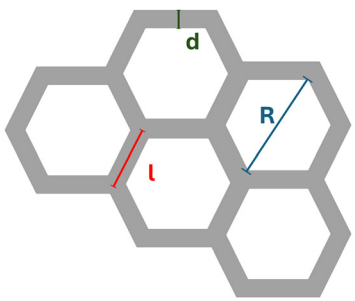

Fig. 1 Honeycomb dimensions used to differentiate patterning. Hole size (R) and strut width (d) were varied with small, medium, and large values as indicated in Table 1. All samples were prepared with the same overall dimensions: 25 × 10 × 0.5 mm (length × width × thickness).

Table 1 Photomask pattern dimensions. All samples were prepared with the same overall dimensions of 25 × 10 × 0.5 mm (length × width × thickness)

Mask name	Hole size (R) (mm)	Hole side (l) (mm)	Strut width (d) (mm)
H1S1	1.3	0.7	0.3
H1S2	1.3	0.7	0.8
H1S3	1.3	0.7	1.5
H2S1	3.0	1.5	0.3
H2S2	3.0	1.5	0.8
H2S3	3.0	1.5	1.5
H3S1	5.0	2.5	0.3
H3S2	5.0	2.5	0.8
H3S3	5.0	2.5	1.5

lations at a loading level of 0.5 wt% relative to the comonomers. These materials were all obtained from Sigma-Aldrich and used as received and without further purification.

Photomasks were purchased from Alpha Chemistry using designs compiled in CAD. Hole and strut sizes were varied between mask types according to Table 1 where R is the diameter of the hexagonal hole and d is the width of the strut between adjacent holes (see, Fig. 1). As expected of a honeycomb (*i.e.*, hexagonal) lattice structure, the ratio of the hole size (R) to hole side (l) was maintained at a value of 2 across all samples. We choose to systematically vary hole size (R), as prior investigations into hydrogel systems[27] highlight a clear relationship between compressive modulus and this parameter. Furthermore, since we hypothesize that strut deformations will play a significant role in geometry based enhancements, the strut width (d) was systematically varied. Each mask was designed to include tabs at either end of the sample to enable mechanical testing (*i.e.*, sufficient contact with specimen when loading into a tensile testing configuration). Nine masks were designed to test each hole and strut size (R and d) combination. The naming scheme for patterns based on hole (*i.e.*, H) and strut (*i.e.*, S) sizes is H(x)–S(y)where x and y have values of 1, 2, or 3 which correspond to the small, medium, and large measurements respectively as highlighted in Table 1. Generally, the patterned area for each specimen was roughly 250 mm^2. Thus, depending on the specific patterning imposed (see Table 1), the number of honeycomb cells (*i.e.* hexagons) in a tested sample varied.

2.2 Experimental methods

Formulation preparation and UV curing. To vary the intrinsic stiffness of the PEG-based networks, differing ratios of PEGMEA : PEGDA were used to vary the cross-link density of the formed network. Specifically, three mass ratios were investigated here: 10 : 90, 20 : 80 and 40 : 60 (PEGMEA : PEGDA). To prepare resin formulations, the appropriate mass of PEGMEA and PEGDA were placed in a vial and allowed to mix *via* magnetic agitation at ambient conditions (→5 min). Then, the appropriate mass of the photoinitator (DMPA) was added at a 0.5 wt% relative to the total monomer mass (combined PEGMEA and PEGDA), and gently mixed until complete dissolution of DMPA was observed (10 min).

Curing molds for photopolymerization were made by sandwiching 0.5 mm thick rubber gaskets between glass slides. Resin formulations as described above were injected into the molds *via* syringe and a photomask was placed on top of the glass slide. Samples were first exposed to a UV light source (ThorLabs Solis 365C, λ = 365 nm, I_o = 10 mW cm^{-2}) for 10–15 seconds. After this initial cure, the photomask was removed and the mold was opened by releasing the top glass slide and any uncured resin was removed with a kimwipe. The remaining sample was then exposed to second curing period (I_o = 100 mW cm^{-2}) for an additional 7 minutes to ensure complete and maximum conversion of the acrylate functionalities and formation of the lattice structure (Fig. 2). After curing, samples were stored in a dark drawer until further testing and analysis.

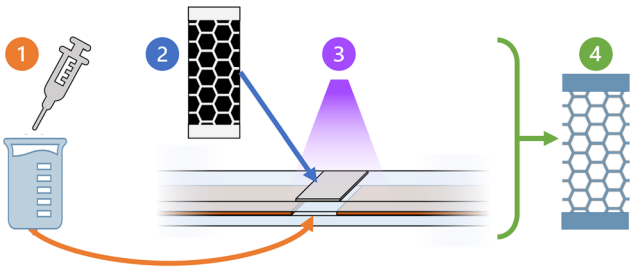

Fig. 2 Curing protocol to develop lattice specimens. Liquid comonomer formulations (1) were injected into a glass mold and the appropriate photomask placed on top (2). Samples were cured for two distinct periods (3). First, a low intensity short cure period (I_o = 10 mW cm^{-2}, 10–15 s) was used to form the lattice structure, after which excess resin was removed from the mold by washing with solvent. The samples were then exposed to a higher intensity curing protocol to complete network polymerization (I_o = 100 mW cm^{-2}, 660 s), after which the final cured specimen was obtained (4).

Dynamic mechanical analysis. A Dynamic Mechanical Analyzer (TA Discovery DMA 850) was used to characterize the mechanical properties of the prepared patterned samples. Strain ramp tests were used to characterize the stress–strain behavior of samples as a function of patterning and intrinsic stiffness. Samples were stretched (0.2 mm min^{-1}) until complete failure or reaching the maximum stretch limit of the instrument (10 mm). Prior to loading of a specimen, the overall sample thickness and width (*i.e.*, without accounting for void spaces due to hexagonal patterning) were measured and inputted into the TRIOS analysis software. The majority of specimens had approximate dimensions of 20 × 10 × 0.5 mm (length × width × thickness). The torque applied to each sample formulation during loading was varied to ensure proper attachment during analysis (*i.e.* avoiding slipping or rupture at the clamps during analysis). Key observations were extracted from the stress–strain analysis, including the location of the first fracture, the nature of crack propagation (catastrophic *vs.* dispersed), strain at failure, and the yield stress (*i.e.*, maximum stress experienced by the sample). The Young's modulus (MPa) was estimated using the slope of the stress–strain data at low strains (0–5% strain, unless otherwise noted). Toughness was calculated by integrating the area under the stress–strain curves. Failure mode was assessed *via* visual inspection. Catastrophic crack propagation was defined as observed rupture of neighboring lattice struts, typically resulting in a break running parallel to the tension clamp. Dispersed crack propagation was defined as observed rupture of non-neighboring lattice struts, *i.e.* struts that were dispersed throughout the sample specimen.

3. Results and discussion

3.1 Overview of pattern-dependent mechanical response

Two handles were explored to investigate failure response in these soft materials: (1) patterning scale of a honeycomb

lattice and (2) intrinsic material stiffness. To address material stiffness, three different mass ratios of the PEGMEA comonomer to PEGDA cross-linker (Fig. S1) were explored: 10 : 90, 20 : 80, and 40 : 60. In this naming convention, the first number refers to the mass fraction of cross-linker included in the comonomer formulation. In a bulk, non-patterned specimen these variations in stiffness have an expected impact on mechanical properties, which is characterized *via* stress–strain analysis (Table 2 and Fig. 3). Specifically, increasing the fraction of cross-linking monomers in the resin formulation corresponds to an increase in Young's Modulus and yield stress. Notably, all base formulations display brittle behavior with sudden and catastrophic failure. Specifically, there is a linear regime at low strains followed by a sudden event that results in a complete break of the sample. Qualitatively, this catastrophic failure is visually marked by a straight break across the specimen that runs roughly parallel to the tension clamp.

Photo-lithography was used to impose patterning onto these network formulations. As highlighted in Fig. 4 for H_xS1 formulations, pattern transfer was crisp with no significant variation in pattern dimensions. Photographs of pattern transfer for H_xS2 and H_xS3 samples are shown in Fig. S2. Stress–strain behavior of patterned specimens was evaluated during tensile deformation, and the behavior for networks based in the 10 : 90 formulation is highlighted in Fig. 5. Two lattice pattern dimensions were systematically varied: pore size and strut width. Each inset (Fig. 5a–c) correspond to a different pore size; strut thickness is indicated by color of the data sets (see legend). In Fig. 5a–c, the bulk (*i.e.* non-patterned data from Fig. 3) is included as a reference.

Specific trends related to failure mode as a function of patterning arise when evaluating Fig. 5. Firstly, staged failure is observed in all samples, indicating individual failure of struts within the lattice structure is observed prior to complete failure (*i.e.* sudden reduction in stress to a 0 value). It is noted that the number of 'stages' of failure experienced by a patterned sample (*i.e.* measured drops in stress prior to complete failure) is dependent on the hole size (R). Given that all samples had similar overall dimensions, the lattices patterned with large hole sizes had a lower absolute number of hexagonal cells in the tested specimen. Thus, the number of individual strut breaks visualized in the stress–strain curve is reduced accordingly going from Fig. 5a–c. There is also a reduction in yield stress across all samples, and this reduction becomes more severe as the porosity (*i.e.* hole size) increases. Furthermore, as pore size increases the patterned network behaves less like a brittle solid (which is the case for the non-patterned control) and transitions to a more ductile material. Specifically in comparing Fig. 5a to Fig. 5c, one can observe how a patterned network achieves a higher strain at break prior to failure. Lastly, a consistent trend regarding strut thickness is observed across all samples: decreasing strut thickness results in a reduced slope of the stress strain curve. Similar trends are observed in the stress–strain behavior of patterned 20 : 80 networks, which is provided in the SI.

In the stiffest network material explored, *i.e.* 40 : 60 formulations (Fig. 6), many of the above noted trends are consistent. Particularly, the transition to more ductile behavior with increasing pore size and decreasing strut width. However, a distinct advantage with patterning in this more stiff and rigid formulation is that in some cases patterning leads to enhanced yield stress compared to the non-patterned (*i.e.* bulk) control. Notably, for pattern H1S2 (pink series, Fig. 6a) yield stress increases by a factor of 1.5 with the imposed pattern, and the strain at break is also increased significantly to roughly 35% (compared to 12% for the non-patterned control).

These impacts of geometry are further supported by visual observation of failure during tensile deformation. Fig. 7a demonstrates how increasing strut width results in more brittle, catastrophic failure (for a 10 : 90 sample with H1S3 geometry). When the strut width gets significantly large, samples behave more like a solid specimen, and a running crack is observed across the specimen parallel to the tension clamp; we define this as catastrophic failure. This is contrasted to Fig. 7b, where strut width is decreased (while maintaining a uniform pore size). Here, random failure of non-neighboring, individual struts is observed, which we define as diffuse

Table 2 Material properties *via* stress–strain analysis for bulk specimens (mean values reported, n = 5). Toughness was estimated by calculating the area under the nominal stress–strain curve

Formulation	Young's modulus (MPa)	Strain at break (%)	Toughness (MPa)
40 : 60	7.09×10^{-2}	12.3	1.52×10^{5}
20 : 80	3.56×10^{-2}	17.7	1.65×10^{5}
10 : 90	1.76×10^{-2}	17.1	4.50×10^{4}

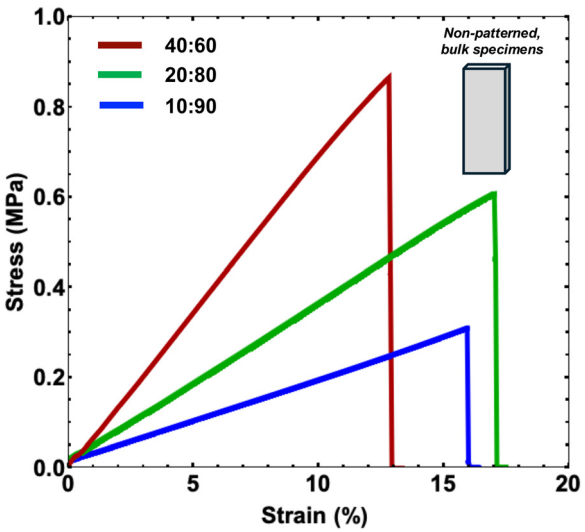

Fig. 3 Stress–strain analysis of bulk specimens without lattice patterning. Bulk specimens have stress–strain behavior related to the cross-link density of the base polymer network (quantitative data presented in Table 2). As expected, increases in cross-link density correlate with a higher Young's Modulus (slope) and lower strain at break.

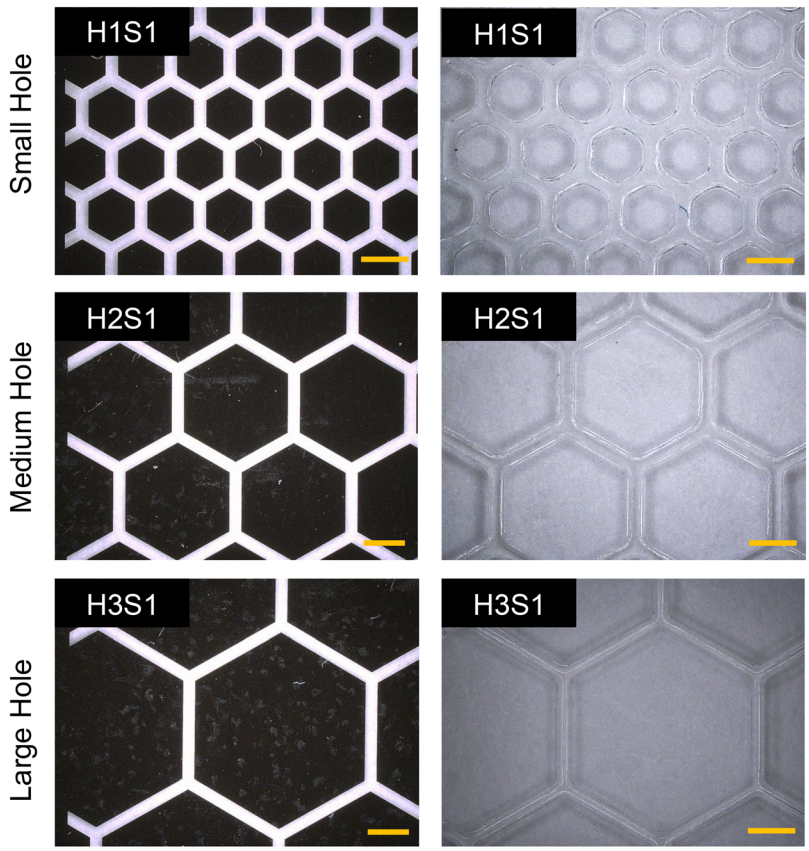

Fig. 4 Optical microscopy highlights differences in lattice dimensions as a function of photomask patterning. Additionally, dimensions are consistent from pattern to formed materials. In all images, the scale bar corresponds to 1 mm.

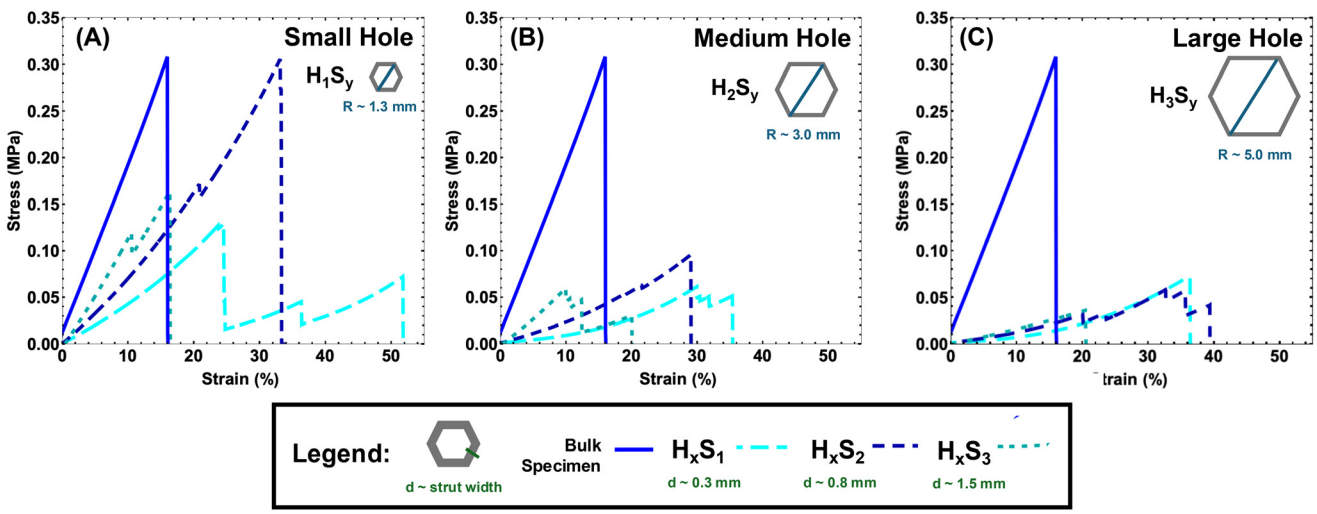

Fig. 5 Stress–strain analysis of patterned specimens based in the 10 : 90 resin formulation. As the general dimension of the pores increases (*i.e.* hole size), the stress–strain behavior evolves from classic brittle behavior to more diffuse types of failure.

failure. This corresponds to the observed 'stages' in patterned stress–strain curves (Fig. 5 and 6).

As demonstrated in prior works,[25,26] when a lattice material is constructed of a purely elastic material – mechanical properties can be predicted based on the lattice geometry (*i.e.* d, R, and l parameters – Table 1). Specifically, the lattice shear modulus (G) and bulk modulus (B) are predicted using the Young's modulus of the base material (Y_o) along with the rela-

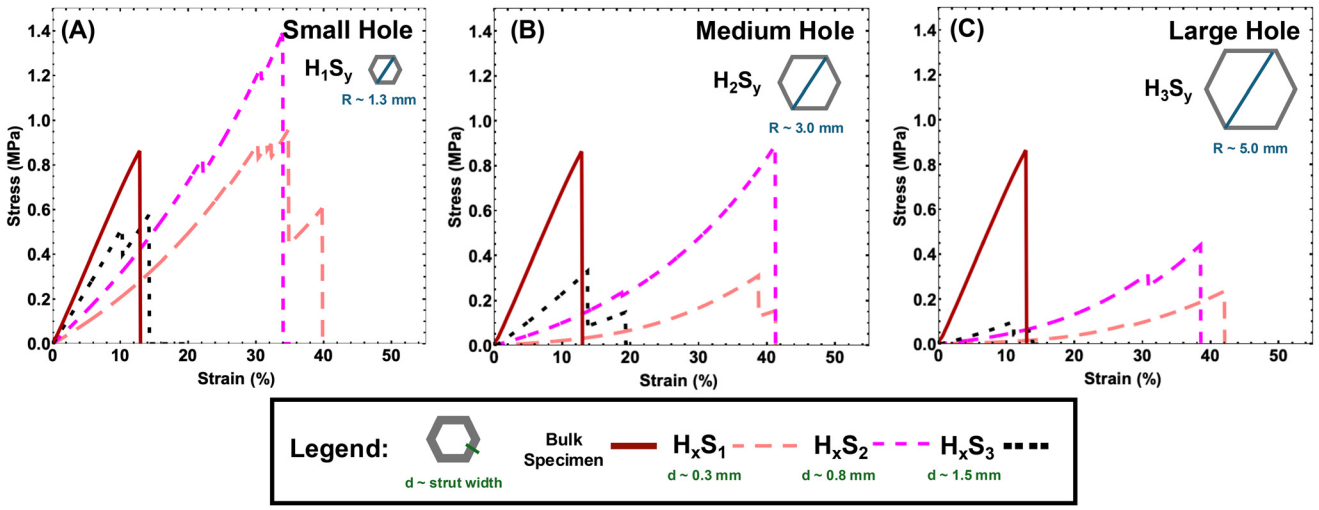

Fig. 6 Stress–strain analysis of patterned specimens based in the 40 : 60 resin formulation. As the general dimension of the pores increases (*i.e.* hole size), the stress–strain behavior evolves from classic brittle behavior to more diffuse types of failure.

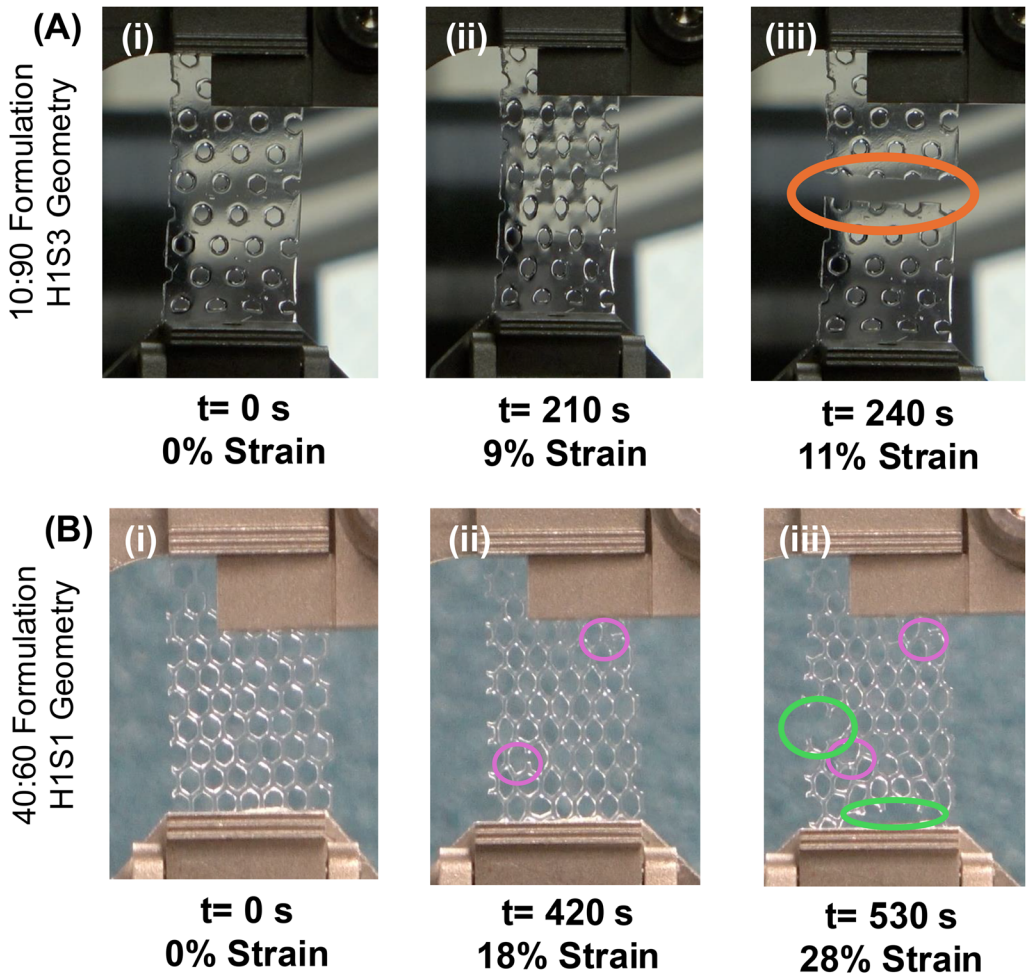

Fig. 7 Visual analysis of failure events and tortuosity support stress–strain data. When strut size (*i.e.*, *d*) is larger, the lattice approaches bulk specimen behavior. During tensile deformation, a propagating crack moves rapidly across the specimen parallel to the tension clamp (A – orange circle), as demonstrated for a 10 : 90 formulation with H1S3 patterning, *i.e.* catastrophic failure. When patterning includes thinner struts with small pores (B – 40 : 60 formulation, H1S1 geometry), dispersed failure was observed. Here, non-neighboring struts fail randomly (purple circles – ii), with eventual failure of additional adjacent lattices (iii).

tive density (ρ^*) of the patterned material *via* eqn (1)–(3). The relative density (ρ^*) represents the fraction of the material that has not been removed when integrating hexagonal pores. As demonstrated previously,[31] in a honeycomb lattice this can be calculated using strut width (d) and length (l). In cases where lattice connections become long and thin (*i.e.*, $d/l \ll 1$), the second term of the relative density equation (eqn (3)) becomes insignificant. Given the explored patterns here, and in particular our H_xS_3 patterns with significant strut widths, this term is included in all calculations of ρ^*. With ρ^*, G and B calculated, a conversion to elastic modulus is straightforward.

$$G = \frac{3}{8}(\rho^*)^3 Y_o \quad (1)$$

$$B = \frac{1}{4}(\rho^*) Y_o \quad (2)$$

$$\rho^* = \frac{2}{\sqrt{3}}\left(\frac{d}{l}\right) - \frac{1}{3}\left(\frac{d}{l}\right)^2 \quad (3)$$

Here, we use the same analysis to compare the measured stress–strain behavior of patterned specimens to that predicted by lattice geometry. The results for a 40 : 60 base network are displayed in Fig. 8 (similar results for 10 : 90 and 20 : 80 formulations are in SI – Fig. S4 and S5). Notably, in both 20 : 80 and 40 : 60 formulations, the experimental results and observed mechanical data significantly 'outperforms' the theoretical predictions when pore size is smaller (*i.e.*, small holes). At larger pore sizes (*i.e.* medium and large hole – Fig. 8b and c), the agreement between theoretical prediction and experimental values are much closer, particularly for the 20 : 80 and 40 : 60 formulations.

This brings up an interesting point and unexpected benefit of lattice patterning. While the staged and delayed failure observed across specimens in this study is expected, the architectural enhancement of mechanical performance, particularly when compared to that predicted of classic brittle materials, is exciting. However, as our data shows, this is very dependent on geometry. Specifically, our analysis highlights how small pore size results in more enhanced performance. However, this analysis is limited to performance at small strains.

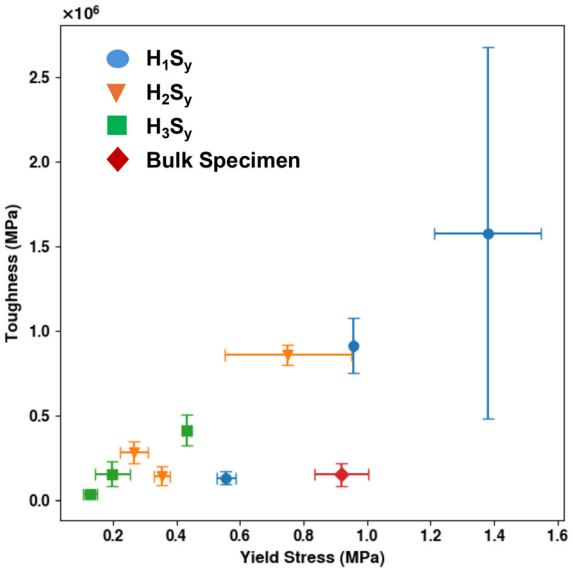

Fig. 9 Hexagonal lattice patterning addresses trade-offs in soft polymer networks. By plotting average yield stress (*i.e.*, strength) *vs.* toughness (*i.e.*, area underneath the stress–strain curves) the influence of patterning, and more specifically pore size is revealed. As pore size decreases (*i.e.*, green to orange to blue series) the trade-off between strength and toughness is significantly reduced. Here this behavior is highlighted for 40 : 60 specimens, with the non-patterned, bulk specimen behavior indicated by the red series. For all data points, the mean value is reported (n = 3) and error bars represent the standard deviation.

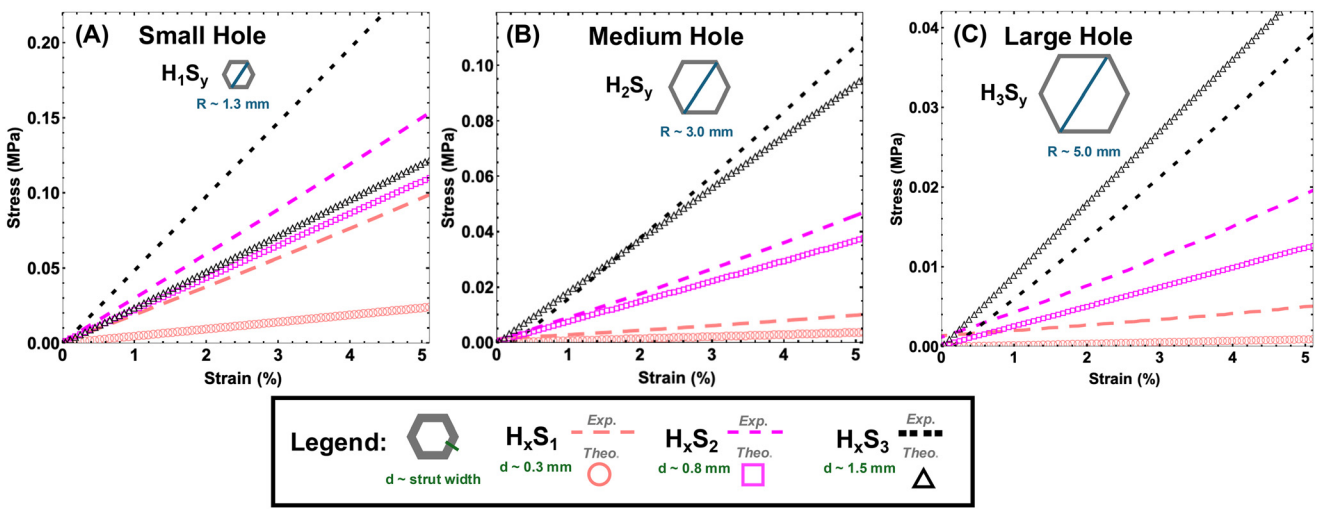

Fig. 8 Stress–strain analysis of patterned specimens based in the 40 : 60 resin formulation at low strains, compared with the theoretical prediction. At low pore sizes (*i.e.* small holes – (A)), the theoretical prediction underestimates mechanical performance. As porosity increases – this shifts. In all figures open series (↘,⇝,≃) correspond to theoretically predicted stress–strain behavior, while dashed series represent experimentally obtained data.

To illustrate the positive effect of patterning over larger deformations (*i.e.*, strains beyond 3–5%), we compared the strength (*i.e.* yield stress) and toughness (*i.e.* area under the nominal stress–strain curve) for all patterned specimens. The tradeoff in these two measures as a function of hexagonal lattice geometry can be visualized in an Ashby plot for each base network formulation. Such an example for a 40 : 60 network is shown in Fig. 9. Here, in a bulk, non-patterned sample toughness is limited due to the brittle nature of the polymer (red series). This is a typical challenge associated with free-radical polymer networks. At large hole sizes (green series), the significant volume of sample removed in creating the porosity results in a significant drop in strength. However, modest increases in toughness are observed with patterning. Most interestingly, patterning with medium and small pore sizes allows for a significant reduction in the toughness *vs.* strength tradeoff. Notably at small pore sizes toughness can increase nearly 10-fold compared to the bulk, non-patterned control, while also achieving a 50% increase in strength. Similar effects of patterning can be observed in the 10 : 90 formulations (Fig. S6); however the relative improvement compared to the bulk control is insignificant in the 20 : 80 formulations.

4. Conclusions

This work demonstrates how honeycomb lattice patterning enhances the mechanical performance of soft polymer networks. Honeycomb lattices comprised of poly(ethylene glycol) photopolymerized networks were formed *via* photolithography, and their response to tensile deformation was investigated. Both the intrinsic material stiffness (*i.e.* cross-link density of the PEG-based network) and honeycomb lattice geometry were varied. All base samples (*i.e.* bulk materials without honeycomb patterning) had behavior characterized by rapid crack propagation and failure at moderate strains (10–20%). However, when hexagonal patterning was imposed, failure transitioned to more diffuse and tortuosity was observed in crack propagation across these specimens. This confirms previously reported behaviors in brittle and composite systems. Most interestingly, our results highlight how patterning can result in enhanced strength and toughness, particularly with smaller, well dispersed honeycomb structures connected by smaller ligaments (*i.e.* struts). Most notably, with the most rigid material explored here a nearly 10-fold increase in toughness and 50% increase in strength was attainable *via* patterning. We hypothesize that this enhancement *via* patterning is due to two contributing factors that can be classified as architectural enhancements. First, the smaller strut size allows for deformations and rotations that are not accessible in the bulk polymer network; with increasing strut size these deformations become restricted. Furthermore, with smaller pores (*i.e.* hexagons) in the honeycomb lattice, tortuosity increases as there are a larger number of deviations and paths available for failure propagation. This architectural enhancement is relevant for applied soft polymer systems, particularly those where both toughness and being light-weight are critical. In particular, emerging technologies such as soft sensors and wearable electronics require withstanding repeated strain and deformations. Using a lattice structure that enhances toughness can address these needs, while also maintaining critical functions (*i.e.* conductivity) even during a diffuse failure process.

Conflicts of interest

There are no conflicts to declare.

Data availability

Data supporting this article have been included as part of the supplementary information (SI). Supplementary information is available. This includes chemical structures of resin constituents, microscope images of initial lattices, additional stress-strain plots and analysis. See DOI: https://doi.org/10.1039/d6lp00046k.

Acknowledgements

During this study, Alyssa VanZanten and Surbhi Punhani-Schillinger were supported by the NSF/DMR (Award 2311697); Hongwei Wu was supported by the NSF/DMR (Award 2311698).

References

1 R. Long, C.-Y. Hui, J. P. Gong and E. Bouchbinder, The fracture of highly deformable soft materials: A tale of two length scales, *Annu. Rev. Condens. Matter Phys.*, 2021, **12**(1), 71–94.
2 C. Creton, 50th anniversary perspective: Networks and gels: Soft but dynamic and tough, *Macromolecules*, 2017, **50**(21), 8297–8316.
3 H. Cao, L. Duan, Y. Zhang, J. Cao and K. Zhang, Current hydrogel advances in physicochemical and biological response-driven biomedical application diversity, *Signal Transduct. Target. Ther.*, 2021, **6**(1), 426.
4 J.-F. Louf, N. B. Lu, M. G. O'Connell, H. J. Cho and S. S. Datta, Under pressure: Hydrogel swelling in a granular medium, *Sci. Adv.*, 2021, **7**(7), eabd2711.
5 C. Majidi, Soft-matter engineering for soft robotics, *Adv. Mater. Technol.*, 2019, **4**(2), 1800477.
6 Z. Wang, X. Zhang, C. Cheng, Y. Liu, D. Qu, P. Shao, J. Jiang and Y. Liu, 3d printing of architectured epoxy-based composite lattices with exceptional strength and toughness, *Composites, Part B*, 2023, **256**, 110653.
7 K.-A. Leslie, R. Doane-Solomon, S. Arora, S. J. Curley, C. Szczepanski and M. M. Driscoll, Gel rupture during dynamic swelling, *Soft Matter*, 2021, 1513–1520.
8 K. Udaka, S. de and Y. Lapitsky, Preparation and timed release properties of selfrupturing gels, *ACS Appl.*

Mater. Interfaces, 2016, **8**(42), 29015–29024. PMID: 27696808.

9 Y. Xiong and O. Kuksenok, Mechanical adaptability of patterns in constrained hydrogel membranes, *Langmuir*, 2021, **37**(16), 4900–4912. PMID: 33844552.

10 A. VanZanten, S. Y. Chen, M. M. Driscoll and C. R. Szczepanski, Unconstrained dynamic gel swelling generates transient surface deformations, *Soft Matter*, 2024, **20**(8), 6742–6753.

11 Z. J. Wang, C. N. Zhu, W. Hong, Z. L. Wu and Q. Zheng, Cooperative deformations of periodically patterned hydrogels, *Sci. Adv.*, 2017, 9.

12 K. Hu, K. Lin, D. Gu, J. Yang, H. Wang and L. Yuan, Mechanical properties and deformation behavior under compressive loading of selective laser melting processed bio-inspired sandwich structures, *Mater. Sci. Eng., A*, 2019, **762**, 138089.

13 M. Ryvkin, V. Slesarenko, A. Cherkaev and S. Rudykh, Faulttolerant elastic–plastic lattice material, *Philos. Trans. R. Soc., A*, 2020, **378**(2162), 20190107.

14 H. Niknam and A. H. Akbarzadeh, Graded lattice structures: Simultaneous enhancement in stiffness and energy absorption, *Mater. Des.*, 2020, **196**, 109129.

15 P. F. Egan, N. R. Khatri, M. A. Parab and A. M. E. Arefin, Mechanics of 3d-printed polymer lattices with varied design and processing strategies, *Polymers*, 2022, **14**(24), 5515.

16 N. Y. Jang, S. R. Park, S. Kim and Y. T. Cho, Mechanically resilient 3d lattices with soft–hard bicontinuous nanostructures via phase-separated interpenetrating composites, *Sci. Rep.*, 2025, **15**(1), 39807.

17 D. Bruson, L. Iuliano and M. Galati, Experimental and numerical mechanical characterisation of additively manufactured polymeric lattice structures under uniaxial tensile load, *Meccanica*, 2025, **60**(3), 647–658.

18 J. Noronha, J. Dash, J. Rogers, M. Leary, M. Brandt and M. Qian, Titanium Multi-Topology Metamaterials with Exceptional Strength, *Adv. Mater.*, 2024, 2308715.

19 S. Fulco, M. K. Budzik, H. Xiao, D. J. Durian and K. T. Turner, Disorder enhances the fracture toughness of 2D mechanical metamaterials, *PNAS Nexus*, 2025, **4**(2), pgaf023. preprint: https://academic.oup.com/pnasnexus/articlepdf/4/2/pgaf023/61663936/pgaf023.pdf.

20 M. C. Fernandes, J. Aizenberg, J. C. Weaver and K. Bertoldi, Mechanically robust lattices inspired by deep-sea glass sponges, *Nat. Mater.*, 2021, **20**(2), 237–241.

21 Q. Zhang, X. Yang, P. Li, G. Huang, S. Feng, C. Shen, B. Han, X. Zhang, F. Jin, F. Xu and T. J. Lu, Bioinspired engineering of honeycomb structure – using nature to inspire human innovation, *Prog. Mater. Sci.*, 2015, **74**, 332–400.

22 H. M. Hameed and H. M. Hasan, Exploring honeycomb structures: A review of their types, general applications, and role in vibration damping and structural stability, *Structures*, 2025, **76**, 108837.

23 S. Zhou, Y. Zhao, K. Zhang, Y. Xun, X. Tao, W. Yan, W. Zhai and J. Ding, Impact-resistant supercapacitor by hydrogel-infused lattice, *Nat. Commun.*, 2024, **15**(1), 6481.

24 L. F. Gockowski, N. D. Dolinski, R. Chavez, N. Cohen, F. Eisenreich, S. Hecht, R. M. McMeeking, C. J. Hawker and M. T. Valentine, Engineering crack tortuosity in printed polymer–polymer composites through ordered pores, *Mater. Horiz.*, 2020, **7**, 1854–1860.

25 M. M. Driscoll, Geometric control of failure behavior in perforated sheets, *Phys. Rev. E: Stat., Nonlinear, Soft Matter Phys.*, 2014, **90**(6), 062404.

26 M. M. Driscoll, B. G. Chen, T. H. Beuman, S. Ulrich, S. R. Nagel and V. Vitelli, The role of rigidity in controlling material failure, *Proc. Natl. Acad. Sci. U. S. A.*, 2016, **113**(39), 10813–10817.

27 D. Yoon, K. N. Eckstein, M. Ruding and P. V. Bayly, Structural tuning of anisotropic mechanical properties in 3d-printed hydrogel lattices, *J. Mech. Behav. Biomed. Mater.*, 2024, **157**, 106625.

28 K. Yao, G. Hong, X. Yuan, W. Kong, P. Xia, Y. Li, Y. Chen, N. Liu, J. He, J. Shi, Z. Hu, Y. Zhou, Z. Xie and Y. He, 3d printing of tough hydrogel scaffolds with functional surface structures for tissue regeneration, *Nano-Micro Lett.*, 2024, **17**(1), 27.

29 S. Pruksawan, Z. A. Chua, Y. T. Chong, T. J. E. Loh, E. L. L. Ng and F. Wang, Smart hydrogel-based mechanical metamaterials: A review, *ACS Appl. Polym. Mater.*, 2024, **6**(20), 12362–12381.

30 S. Wang, J. Wang, Y. Xu, W. Zhang and J. Zhu, Compressive behavior and energy absorption of polymeric lattice structures made by additive manufacturing, *Front. Mech. Eng.*, 2020, **15**(2), 319–327.

31 L. J. Gibson and M. F. Ashby, *Cellular solids: Structure and properties*, Cambridge University Press, Cambridge, UK, 2nd edition, 1997.